Smart RFID label with a printed multisensor platform for environmental monitoring

2016 Flex. Print. Electron. 1 025003

(http://iopscience.iop.org/2058-8585/1/2/025003)

Flexible and Printed Electronics

RECEIVED
26 January 2016

REVISED
11 April 2016

ACCEPTED FOR PUBLICATION
18 April 2016

PUBLISHED
17 May 2016

PAPER

Smart RFID label with a printed multisensor platform for environmental monitoring

A Vásquez Quintero[1], F Molina-Lopez[1], E C P Smits[2], E Danesh[3], J van den Brand[2], K Persaud[3], A Oprea[4], N Barsan[4], U Weimar[4], N F de Rooij[1] and D Briand[1]

[1] Ecole Polytechnique Fédérale de Lausanne (EPFL), Institute of Microengineering (IMT), Sensors, Actuators and Microsystems Laboratory (SAMLAB). Rue de la Maladière 71b, CH-2002, Neuchâtel, Switzerland
[2] Holst Centre/TNO, High Tech Campus 31, 5656AE Eindhoven, The Netherlands
[3] The University of Manchester, School of Chemical Engineering & Analytical Science, Manchester M13 9PL, UK
[4] University of Tübingen, Institute of Physical and Theoretical Chemistry, Auf der Morgenstelle 75, 72076 Tübingen, Germany

E-mail: andres.vasquez@alumni.epfl.ch

Keywords: printed chemical sensors, inkjet printing, foil-to-foil integration, RFID smart labels, polymeric substrate, environmental variables

Abstract

This work reports on the design, fabrication and characterization of an inkjet-printed multisensing platform on flexible polymeric substrates integrated into a printed semi-passive high frequency radio frequency identification (HF RFID) smart label. The printed platform was integrated after fabrication to the main RFID carrier, which contained an NFC RFID chip, a microprocessor, a readout frontend and a screen-printed circuitry and antenna. The multisensing platform has channels for capacitive vapor detection (i.e. humidity), two channels for resistive-based vapor detection (i.e. ammonia) with heating capability, and one resistive channel for temperature detection (RTD). A modular approach was employed where the sensing platform was integrated to the base RFID label carrier using foil-to-foil integration techniques compatible with large area fabrication. Besides wireless communication, the semi-passive label possesses data logging and the possibility of measuring all the sensors simultaneously through a direct readout circuitry. In addition to individual sensor characterization, the full functionality of the smart label was successfully demonstrated by measuring different temperature, humidity and ammonia levels.

1. Introduction

Wireless sensing radio frequency identification (RFID) systems have recently started to be commercialized in order to enable the monitoring of environmental variables in logistics applications like, for instance, cold chain supply. The motivation towards the use of such systems is their potential to reduce waste during transportation [1]. However, current RFID devices are bulky and relatively expensive, restricting their implementation into large scale applications, such as environmental monitoring in logistics. The vast majority of the commercially available RFID based sensor systems includes only a temperature sensor, with the exception of only a few that have an integrated a humidity sensor. Some experimental models of printed RFID tags with sensors have been demonstrated recently [2–5], while few others have incorporated specific environmental sensors together (i.e. temperature, humidity and ammonia) [6, 7]. Nevertheless, current sensor fabrication technology for smart labels either incorporates Si-based transducers [8, 9] or employs clean room processes (i.e. photolithography). Notably, the company Thinfilm Electronics, leading the printing technology of smart labels, has devised a fully printed solution with printed memory, display and wireless interface, however limited to only temperature sensing (i.e. printed silicon-based sensor from the company PST). Going beyond the state of the art, we worked to combine a printed RFID label with a fully printed multisensor platform for environmental monitoring.

In the last few years, there has been significant focus on the development of flexible environmental sensors that are directly printed on polymeric substrates [10, 11]. Besides their large area processing

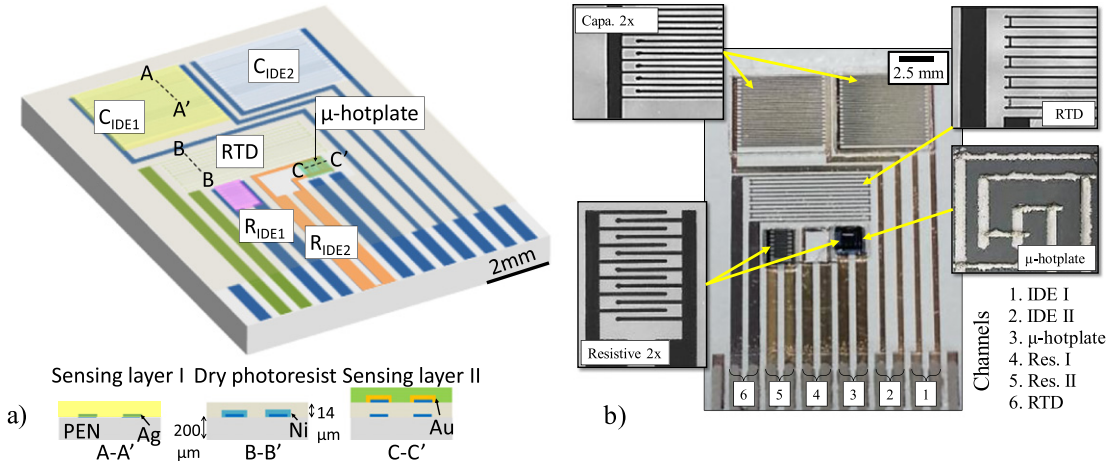

Figure 1. (a) Sketch of the platform describing the distribution and size of every component and different layers employed and (b) optical microscope pictures of the multisensor platform showing the six different channels after fabrication.

compatibility, such sensors offer several advantages compared to their silicon counterparts, even if the overall performances of the former may be lower at present. These potential advantages encompass low manufacturing costs, less stringent size constraints, easy distribution in arrays, light weight, flexibility and conformability, among others. In previous publications, we demonstrated the feasibility of printing, on polymeric substrates, resistance temperature detectors (RTD) for temperature monitoring [12], capacitive sensors with cellulose acetate butyrate (CAB) for humidity sensing [11], and chemiresistive sensors with conductive polyaniline (PANI)/carbon nanocomposite for ammonia (NH_3) sensing (i.e. with heating recovering capabilities) [13, 14]. Here, we present a combination of these sensors on a single polymeric platform and its integration onto a printed HF RFID label using techniques compatible with large area manufacturing [15]. The smart sensing system was characterized through sensitivity and cross sensitivity measurements. The data have been monitored using the RFID communication protocol, and acquired on the local tag memory. From there, the information was retrieved for later processing. The combination of several sensors onto the same platform allows the reciprocal correction of the device output parameters and therefore enhances its applicability. Temperature, humidity and ammonia were chosen to exemplify the smart label sensing capabilities due to their relevance for many monitoring applications, notably in the food logistic chains.

In this paper we report on the realization and the functional performance of a semi-passive HF RFID smart label with multisensing capabilities conceived on flexible plastic substrates, mainly by printing techniques (i.e. inkjet and screen printing). Semi-passive HF RFID uses an on-board power source (i.e. a battery) for sensor recording and data management, and uses the passive backscatter principle to communicate with the reader [16]. In order to increase the efficiency and the production yield, the manufacturing of the base label (i.e. electronic circuitry, battery, passive and active components as well as RFID antenna) and that of the flexible sensing platform were scheduled in separate processes, the two parts being merged together in the last step only. Moreover, the chemically functionalized printed-sensors were tested and calibrated before their final integration on the tag. Making use of different transducing principles (i.e. capacitive and resistive), the inkjet-printed multisensor platform combines several transducers and sensing layers for the simultaneous detection of water vapor, ammonia, and temperature.

This paper is organized as follows: the design and fabrication of the inkjet-printed multisensor platform is presented in section 2, while the fabrication of the RFID smart label and the platform integration is presented in section 3. The characterization of the environmental sensors (i.e. temperature, humidity and ammonia) is presented in section 4. Finally, the conclusions and perspectives of this work are presented in section 5.

2. Inkjet-printed multisensor platform

2.1. Design and layout

The inkjet-printed multisensor platform includes two capacitive transducers, two resistive transducers, one micro hotplate and one resistance temperature detector (RTD), as shown in figure 1. The design of the multisensory platform was based on a double metallization level of printed silver layers, separated by a very homogeneous polymeric dielectric film (i.e. laminated dry film photoresist—DP). The DP PerMX3050® from DuPont was used as well as a protection layer, which increases the robustness of the printed metallic tracks upon bending. The first metallic layer includes the interdigitated capacitor electrodes (IDEs), the RTD, a

set of smaller IDEs for the resistive sensing and the heater of the micro hotplate. The second metallic layer was printed directly on top of the DP and includes the second set of IDEs for resistive sensing (i.e. above the micro hotplate). The printed components can be selectively electroplated (i.e. to improve their stability and performance), while the platform was integrated to the main RFID carrier with large-area compatible lamination techniques (i.e. foil-to-foil).

The IDEs were composed of 36 fingers, 5 mm long, with a pitch of 120 μm and within an area of 5.1 $\times$ 4.2 mm^2. The small IDE without heater has 14 fingers (1 mm long) with a total area of 1.2 $\times$ 1.6 mm^2. The micro hotplate stack was composed of a double meander heater with a length of 7.5 mm (with an area of 1 mm^2), a 14 μm thick DP dielectric layer and IDEs aligned on top. The latter IDE was formed by 8 fingers of 0.8 mm in length with a pitch of 120 μm (covering an area of 1 mm^2). Finally, the RTD was devised with six meanders of 240 μm pitch and 6.7 mm long (i.e. total length of 83.3 mm and occupying an area of 7.3 $\times$ 2.7 mm^2). Figure 1(a) shows a sketch of the platform with its different components and relevant cross-sections indicating the materials and thicknesses of every layer. The contact pads were designed to be compatible with zero-insertion-force (ZIF) connectors of 1 mm pitch (i.e. 700 μm wide with 300 μm of spacing), to test them before the integration. The silver-based printed layer (i.e. 200 nm thick) can be used as a seeding layer for the electroplating of nickel and/or gold to passivate the electrodes, in order to increase the temperature coefficient of resistance (TCR) of the RTD and to improve the robustness of the micro hotplate. As proof of concept in this paper, one of the capacitive IDE transducers was used to sense humidity (i.e. the second set can be used to measure humidity in differential mode and/or other analyte). One of the resistive transducers in combination with the micro hotplate was used to sense ammonia (i.e. the second set can be used to measure other analyte). The combination of capacitive, resistive and RTD transducers was used to measure simultaneously humidity, ammonia and temperature, respectively.

2.2. Fabrication

The multisensor platform process flow consisted of four main steps, depicted in figure 2. First, the two large capacitive structures, RTD, heater of the micro hotplate, one resistive IDE channel structure and all contact pads were inkjet-printed with the Jet EMD506 silver ink using the Dimatix DMP-2800 (10 pl drop cartridges) onto PEN substrates (Teonex QF65A), as shown in figure 2(a). After annealing the structure for 3 h at 180 °C, the RTD was electroplated with 1 μm of nickel in order to take advantage of a higher temperature coefficient of resistance (TCR) to improve its sensitivity. The IDE capacitance and micro hotplate resistance values were measured to be 3.5 $\pm$ 0.2 pF and 150 $\pm$ 4 Ω, respectively, while the RTD resistance value resulted in a nominal value of 1.0 $\pm$ 0.1 kΩ before the Ni electroplating and 500 $\pm$ 35 Ω afterwards (error value represents standard deviation from three measured samples). The complete characterization of the Ag inkjet-printed lines (i.e. SEM and white light interferometer images) was presented in [11], which resulted in a thickness of 200 nm and 1 μm before and after the Ni electroplating, respectively.

Figure 2(b) illustrates the lamination and patterning of the dielectric DP film using standard photolithography. The DP was specially patterned to open windows on top of the sensors (i.e. excluding the RTD) for further functionalization and electrical contacts. The complete processing steps and properties of the DP are described in [17].

The second metallic layer included an IDE set dedicated to the resistive ammonia sensor. It was printed directly onto the DP above the micro hotplate, as shown in figure 2(c). This structure was electrodeposited with 0.5 μm of Au (figure 2(d)) in order to improve its chemical stability, especially when in contact with the PANI-based ammonia sensing layer. The chemoresistive devices resulted in a final resistance in the range of several MΩ after the respective coating of the sensing layer. Au electrodeposition could also be used on the rest of the transducers in order to increase their stability in time, as well as Ni or Au electrodeposition on the heater of the micro hotplate to increase its reliability [12, 18]. The final printed structure is depicted in figure 1(b), indicating all the transducers and their respective channels.

2.3. Sensing layers

2.3.1. Humidity sensing layer

The humidity sensing layer was fabricated by dissolving 65 mg of CAB in 4 ml of hexyl acetate (purity >99% from Sigma Aldrich). The dissolved polymer was subsequently inkjet-printed onto only one of the IDEs. After inkjet printing, the solution was dried for 30 min at 85 °C in a convection oven, resulting in a 8 $\pm$ 1 μm-thick layer after printing 25 consecutive (overlapping) layers (optimization taken from reference [11]) and a measured capacitance value of 4.1$\pm$ 0.2 pF. Although relatively high amount of layers were printed, inkjet printing was selected as the deposition method for CAB due to the high precision achieved for the thickness of the layer [11].

2.3.2. Ammonia sensing layer

We recently showed that doped PANI thin films fabricated by the vapor-phase deposition polymerization method could detect NH_3 vapor in sub-ppm concentration range in air, both under dry as well as humid conditions [18]. Polyaniline however, has generally been considered as an insoluble polymer [19] hindering advantageous deposition techniques such as spin coating and inkjet printing for fabrication of

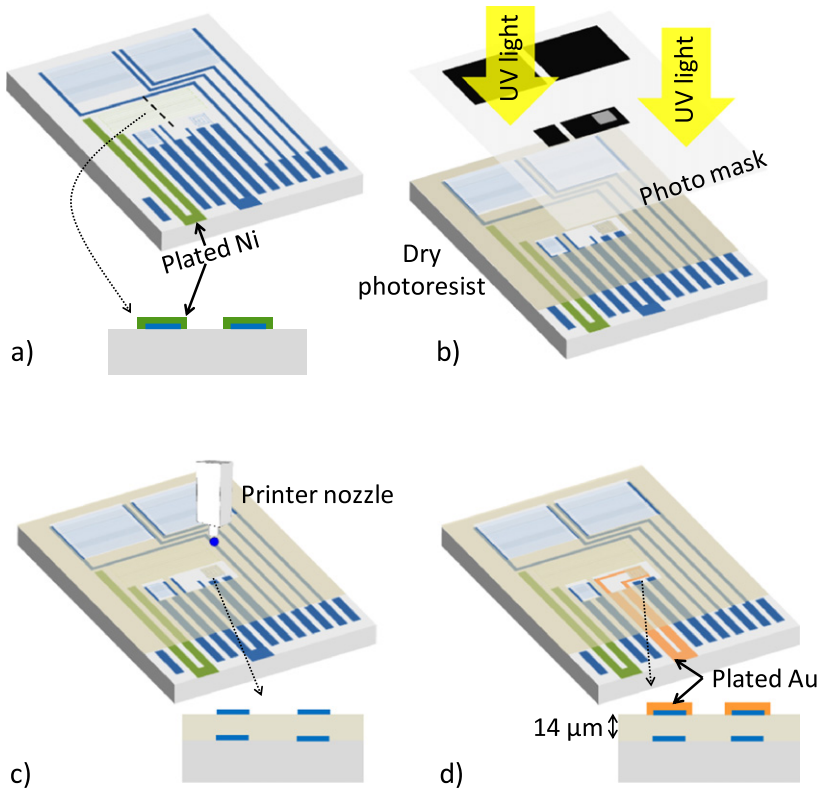

Figure 2. Fabrication steps of the multisensor platform. (a) Inkjet printing and Ni plating of the first metallic layer on the PEN substrate, which includes two capacitive transducers, a resistive one, an RTD and a micro hotplate. (b) Photolithography processing of a DP layer to isolate the second metallic layer and to reinforce/protect the first one. (c) Inkjet printing of the second metallic layer, which includes the resistive sensor IDE on top of the micro hotplate. (d) Gold plating of the IDE on top of the micro hotplate to enhance chemical stability.

PANI-based sensors. Great effort has been made to enhance the solution processability of polyaniline in its doped state (emeraldine salt). In this study, the counter-ion induced processability concept [20] was employed to prepare PANI solution in an aprotic solvent. The targeted material was further modified towards a carbon/PANI nanocomposite [21] by incorporating surface-modified carbon nanoparticles into the precursor solution, in order to improve its electrical and ammonia sensing properties. The ammonia sensing layer was fabricated as described elsewhere [21], by mixing polyaniline emeraldine base (EB, MW ~ 10 000 g mol^{-1}), sulfosuccinic acid (SSA solution, 70 wt.% in water), surface-modified carbon black (CB, 20 wt.% polyaniline on carbon black composite) and n-methyl pyrrolidone (NMP). The final composite had 20 wt.% CB and 80 wt.% PANI, which was found as optimum in our previous publication [21], which is in good agreement with other published studies in literature [22]. All the chemicals were used as received from Sigma Aldrich without further purification. The sensing layer was deposited by drop casting (~1 μl) on the IDEs, and left to dry under air flow at ~20 °C and 70% relative humidity [21]. Finally, the layer was annealed at 120 °C for 30 min to evaporate the residual solvents.

The sulfosuccinic acid acts as a multifunctional dopant which, in the same time, dopes and solubilizes emeraldine base in NMP. The sulfonic acid group in the SSA is believed to protonate nitrogen atoms on imine sites [23], converting emeraldine base to the electrically conducting emeraldine salt form, while the two carboxylic acid groups produce strong hydrogen bonds with NMP, assisting the dissolution [24]. According to the manufacturer, the CB nanoparticles (d ~ 40 nm) used in this study possess a core–shell structure with carbon black as the core and a thin polyaniline coating as the surrounding shell which serves mainly as an electrical interconnection between the polymer matrix and the carbon black particles. This causes fine dispersion and uniform distribution of the nanoparticles in the composite while preserving the electrical properties of the pristine carbon nanoparticles. Achieving a homogeneous hybrid mixture is crucial in order to fabricate uniform sensing layers with good reproducibility.

3. Printed and hybrid RFID label

3.1. Label design and its components

The RFID label's circuitry was screen-printed onto a 125 μm thick PEN substrate (i.e. Teonex® Q65FA from DuPont Teijin Films™) with two metal layers and one

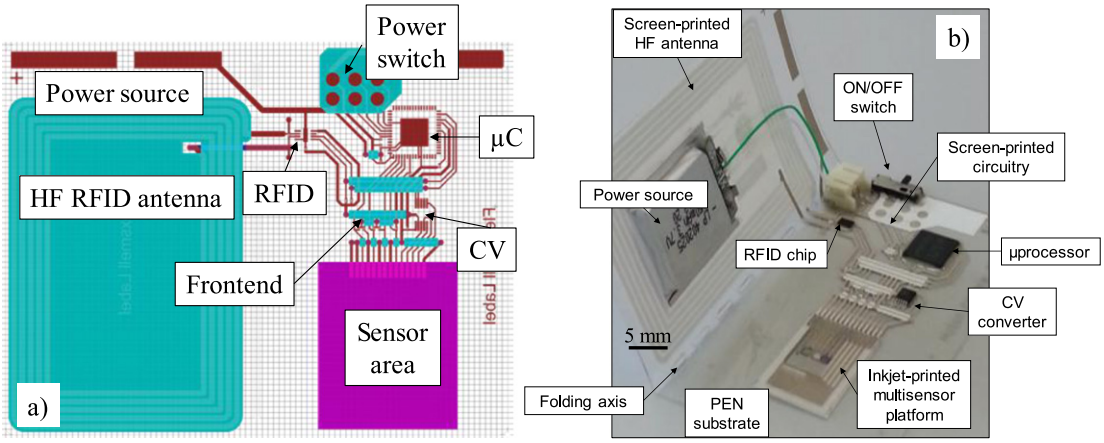

Figure 3. (a) Layout of the FlexSmell high frequency RFID smart label, indicating the main components and architecture and (b) picture of the final assembly of the RFID smart label (half folded), including the inkjet-printed multisensor platform.

dielectric architecture. The three printing steps used the 400 mesh screen type SD40/25 with a 10 μm emulsion thickness. The two metal layers used micron flake silver-based paste 5064 from DuPont with a typical sheet resistance of 12 mΩ/sq/mil and a typical print thickness of 6 μm for one printing pass. The above-mentioned materials and parameters gave sufficient conductivity in the antenna (i.e. total resistance of 50 Ω). If a thicker antenna is needed, a thicker screen or higher mesh can be used, however the printing resolution will be reduced (i.e. bonding pads of 200 μm need to be considered for the SMD components). The printed ink was cured in a convection oven at 150 °C for 30 min, resulting in a thickness of 35 $\pm$ 4 μm. Required for bridging the antenna and several circuit connections, the bridges were fabricated by screen printing the dielectric paste 5704 from DuPont and cured in an oven at 150 °C for 30 min. A total of three printing passes were used (i.e. with a typical thickness of 6 μm/layer) in order to reduce the risk of pin holes which would provoke short circuits. Two passes could be sufficient by using a thicker mesh or an UV-curable dielectric material (i.e. higher viscosity).

The RFID antenna was conceived with a square shape multi-loop design considering a resonating frequency of 13.56 MHz and a chip internal tuning capacitance of 27.5 pF. Using equation (1), the total inductance of the antenna was calculated to be 5.01 μH. Such inductance value in combination with the software 'Antenna_ST_desing_AN2866.exe' from ST Microelectronics were used to define the optimal dimensions of the squared-shape antenna, shown in figure 3.

$$L_{\text{ant}} = \frac{1}{(2\mu \times f_0)^2 \cdot C_{\text{tun}}} = \frac{1}{(2\pi \times 13.56\ \text{MHz})^2 \cdot 27.5\ \text{pF}} = 5.01\ \mu H \quad (1)$$

Where, f_0 is the RFID resonating frequency, C_{tun} is the tuning capacitance of the RFID chip and L_{ant} is the calculated inductance of the antenna.

The label consists of an RF coil antenna, metallization circuitry, bridges and integration pads for discrete components as well as an interface for the multisensor platform. The labels were fabricated on a flat A4 surface and then detached as single pieces using a 355 nm ns laser (Coherent Avia, in combination with a Galvano scanner system). The label, with a surface of 7 $\times$ 9 cm^2, can be further folded in order to achieve the dimensions of a credit card, which is 4.5 $\times$ 7 cm^2. The layout and the location of the principal components such as the multisensor platform, RFID chip, microcontroller, HF coil antenna, frontend components (i.e. capacitance to voltage converter and voltage divider circuitry), power switch and battery electrodes are illustrated in figures 3(a) and (b). It should be noted that the ON/OFF switch here was used for demonstration purposes and that the final assembly was activated by direct contact of the battery (i.e. 150 mAh at 3.9 V battery—PK Cell from Adafruit) with the supply pads on the foil (labelled with 'Power source' in figure 3(a)).

The RFID label was operated in an autonomous manner through the use of a MSP430F1611 microcontroller from Texas Instruments, chosen due to its low power functionality, integrated temperature sensor (potentially useful to compensate other sensors on-tag) and because of its highly sensitive analog-to-digital converter (ADC). The wireless interface was performed through the RFID chip STM24LR64 with dual interface eeprom from ST Microelectronics (compliant with the ISO 15693 standard). The dual interface, both with RFID and I^{2}C, was used to power the chip from the RF field and communicate directly to the microcontroller, respectively. The humidity IDE transducers were interfaced to the microcontroller via the capacitive frontend chip AD7150 from Analog devices, since it provides a two-channel independent and calibrated output; very useful when reading different sensors, in addition to its sensitivity in the desired capacitive range (i.e. pF signal from sensors).

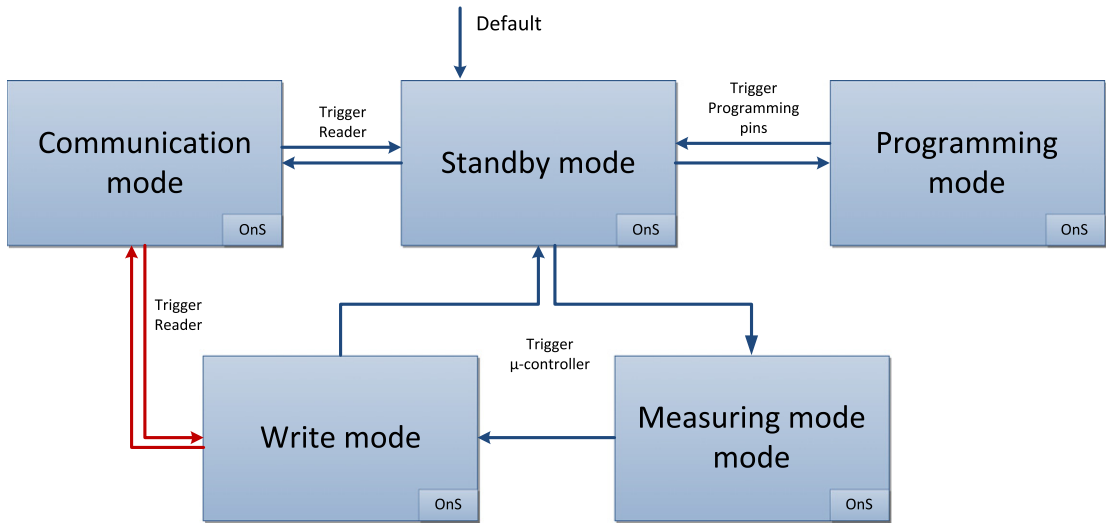

Figure 4. Modes in states diagram in the ON state (OnS) of the FlexSmell label.

The readout was activated by the microcontroller and was made accessible over an I^2C bus. In contrast, each resistive sensor was connected in a voltage divider configuration with a defined matching resistor (i.e. in the order of MΩ for the ammonia sensor and kΩ for the RTD) to the analog-to-digital converter of the microcontroller. The voltage divider configuration was biased by the microcontroller (i.e. 3 V when the battery is fully charged) with a conversion resolution of $3\ V/2^{12}\ bit = 0.73\ mV\ bit^{-1}$.

The chips and discrete components were integrated using the semi-automatic bonder Tresky T3200® and the isotropic conductive adhesive (ICA) CE 3103 WLV from Henkel®. The chips could also be integrated at the bare die format (thinned down if necessary) using a combination of flip-chip techniques and iso-/anisotropic conductive adhesives [25].

The general operation of the smart label can be described in five function modes: programming mode, standby mode, measuring mode, write mode and communication mode. Figure 4 depicts the relationship between the five operation modes. In programming mode only the microcontroller was addressed while the firmware was uploaded. The system returned to standby mode when the programming pins were removed, or to the off state if no external power was supplied. In standby mode the microcontroller enters the sleeping mode allowing only the internal clock to function. Both the NFC chip and capacitance readout chip were in the off state. A trigger of the internal clock of the microcontroller will exit the standby mode and put the system in the measuring mode. In measuring mode the microcontroller reads out the sensors one by one, while the data (i.e. raw output of the AD converter and a time stamp) are stored temporarily on its memory. In write mode the data stored in the microcontroller is written in the memory of the dual interface eeprom over an I^2C bus. Finally, in communication mode an external reader reads out the dual interface eeprom memory with energy supplied through the RF link by the reader. The human interface of the smart label includes different configuration settings regarding the operation mode (i.e. live-mode: data are displayed on the PC screen as it is measured; logging-mode: saving the data on the RFID memory for later retrieval). Measuring intervals can be defined with a maximum storage capacity of 6000 points (i.e. including data from all the sensors). Such settings, as well as the gathering and saving of the data, are possible through a wireless interface using the commercial RFID reader M24LR-DISCOVERY from ST Microelectronics and a custom made LabVIEW interface.

3.2. Foil-to-foil integration of the multisensor platform

After screen-printing the circuit interconnections and RFID antenna, the first layer of pressure sensitive adhesive (PSA) ARClear 8932 (50 μm-thick) from Adhesive Research® was laser-ablated to open 200 μm wide vias and access windows for the environmental sensors, and bonded to the main PEN substrate, as shown in figures 5(a) and 6(a). After the lamination, the interconnection vias were filled with isotropic conductive adhesive (ICA) CE 3103 WLV from Henkel® [15], using stencil printing (figure 6(b)). The multisensor platform, inkjet-printed in a parallel process, as described in section 2.2, was integrated into the main PEN carrier using the flip-chip approach previously demonstrated in [15] (figures 5(b) and 6(c)). The PSA was used to mechanically attach the platform to the main substrate. Thanks to the relatively big interconnection pads (i.e. pitch of 1 mm) the alignment was performed by hand through an optical microscope. At this point, the ICA was cured in a convection oven for 1 h at 85 °C. A second pre-

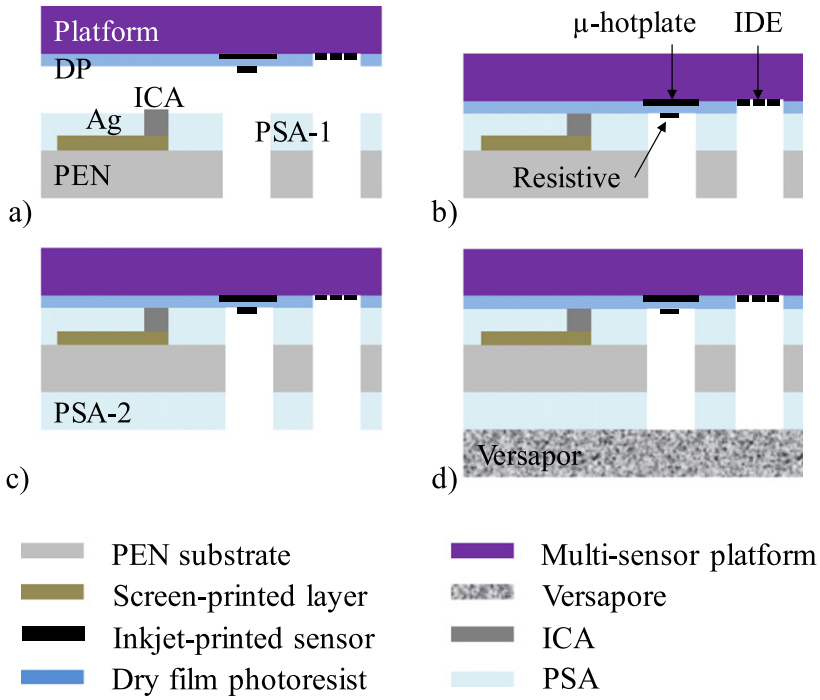

Figure 5. Fabrication steps of the multisensor platform integration. (a) Laser ablation of the first PSA layer, lamination onto the main carrier, and filling the blinded vias with ICA. (b) Alignment and lamination of the multisensor platform onto the PEN main carrier. (c) Lamination of the second PSA layer on the bottom side of the carrier. (d) Lamination of the Versapor porous membrane to fully encapsulate the sensors while protecting them.

patterned layer of PSA was bonded on the bottom side of the label (figure 5(c)) in order to fix a 135 μm thick acrylic copolymer porous membrane (i.e. Verspor® 10000R from PALL™) [12], as shown in figures 5(d) and 6(d). The semi permeable membrane should allow the analytes (i.e. water vapor, ammonia) to reach the sensors while protecting them from handling and/or dust contamination.

4. Results and discussion

The performance of the sensing materials, multisensor platform, and full smart sensing label has been consecutively investigated under vapor exposure. The experiments have been scheduled as evaluation steps towards final device architecture and functionality. In agreement with the research aim, three groups of ambient characteristics have been envisioned: temperature, humidity and gaseous analytes (i.e. NH_3).

An overview over the smart sensing tag capabilities is given by the screen-shot of the main window of the LabVIEW user interface as shown in figure 7. The three panels represent the graphical output of the raw data acquired by the system as follows: (left) the resistance of the RTD dedicated to temperature measurement; (center) capacitive, the IDE capacitive transducer coated with a CAB layer for humidity sensing; (right) the resistance with PANI-based sensing layer for NH_3 detection. The data depicted in figure 7 illustrate a constant temperature of 25 °C, a staircase humidity variation from 30 to 50% R.H. (30, 40 and 50%), and the output of the NH_3 sensor for ammonia concentrations ranging from 0 ppm to 15 ppm (0, 5, 10 and 15 ppm steps) for 15 h. The individual sensor and system characterization will be described in the sections hereafter.

4.1. Temperature sensor characterization

The RDT sensor plays a double role in the developed concept. On one hand, it delivers one of the main tag output parameters (i.e. the environment temperature). On the other hand, the temperature value can be used for the compensation of the other output parameters (that is for humidity and NH_3 correct evaluation). For instance sensitivity of both sensing layers (i.e. CAB partition coefficient for humidity and PANI partition coefficient for NH_3) as well as the ambient absolute humidity (Antoine law) strongly depend on temperature. Although not implemented yet in the actual version of the tag software (out of the scope of this paper), the compensation, calibration as well as graphical user interface can be integrated in the firmware of the label itself through proper coding.

Temperature tests were performed in the climatic chamber SH-661 from the company Espec (Benchtop temperature and humidity chamber) and were able to reproduce controlled temperature and humidity conditions with a precision of 0.5 °C and 2% R.H., respectively. The temperature characterization occurred under different heating and cooling conditions (i.e. at 40%R.H. between −10 °C and 80 °C with steps of

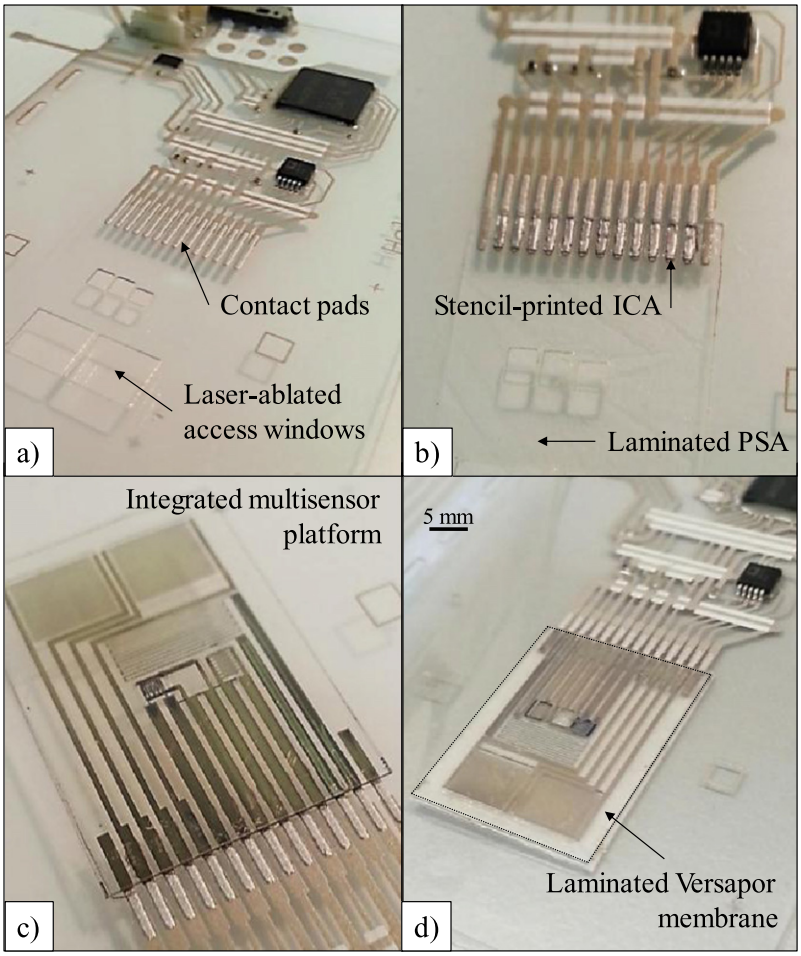

Figure 6. Pictures of the multisensor platform integration. (a) Laser-ablated access windows on PEN main carrier. (b) Laminated PSA with stencil-printed ICA at the connection pads. (c) Integrated multisensor platform. (d) Laminated Versapor membrane on the back side of the stack.

10 °C for the TCR calibration and steps of 1 °C for the resolution determination), as indicated in figure 8(a). For the temperature calibration curves, a staircase temperature profile was chosen in order to avoid the errors that could be introduced by the settling time of the chamber. Figure 8(b) shows the calibration curves of the printed RTD, indicating up- and down-sweep TCRs of 1100 and 1129 ppm K^{-1}, respectively. Although the linearity was maintained, the measured TCR values were lower than the ones reported previously [12]. This could be improved by optimal Ni plating and/or a prolonged ink annealing process.

The resistance of the RTD was measured by using a voltage divider (VD) with its output voltage directly connected to the analog-to-digital (ADC) converter of the microprocessor (i.e. 12 bit resolution). At the maximum reading voltage (i.e. 3 V provided by the microcontroller when the main battery is fully charged) the conversion resolution was calculated to be $3\,V/2^{12}\,bit = 0.73\,mV\,bit^{-1}$. Considering a temperature operational range between −10 °C and 80 °C, the RTD values were measured to be between 500 Ω and 550 Ω (figure 8). This corresponds to an output voltage from the VD between 1.5 V and 1.571 V. This range provides a quite linear response, as expected from the VD design, with a maximum variation of 0.75 mV for resistance steps of 0.5 Ω. The latter value allows us to estimate the maximum resolution of the actual system to be 1 °C (i.e. limited by the ADC resolution), that is, 0.1% of the nominal RTD value at room temperature. The achieved resolution of ∼1 °C satisfies for a general purpose monitoring system.

4.2. Humidity sensor characterization

Humidity characterization was performed using the climatic chamber SH-661 from Espec. Figure 9(a) shows the dynamic response of the humidity sensor when coated with a CAB sensing layer (black squares). The measured RTD resistance values corresponding to the ambient temperature are shown in the right axis in figure 9(a) (blue solid line). From figure 9(a) the response and recovery times can be evaluated. Response times of 5.43 min and 8.05 min were calculated from 20% to 40% and from 40% to 60%, respectively; while recovery times of 5.75 min and 6.64 min were calculated from 60% to 40% and from 40% to 20%, respectively. Both response and recovery

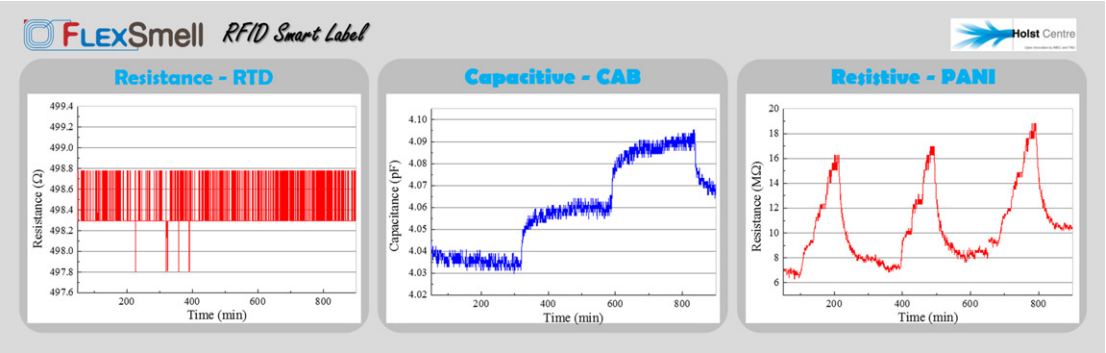

Figure 7. Overview of the measured data after being retrieved from the label and visualized with the LabVIEW user interface. The screenshot shows the raw data from a set of measurements where the temperature was kept constant at 25 °C while the humidity and ammonia concentrations have been changed stepwise (30%, 40% and 50% R.H., and 0, 5, 10 and 15 ppm NH_3 for each humidity level).

times are comparable with other similar values reported in the literature [11, 12].

The temperature plot indicates no cross sensitivity of the RTD towards humidity, which is required for an accurate temperature measurement and efficient correction of the humidity sensor signal for temperature variations. The immunity of the temperature sensor against humidity was achieved thanks to the low water vapor permeability of the DP protection layer deposited on top of the RTD structure, which prevented the direct contact of water vapor and the RTD structure. The absence of cross sensitivity improves our previous results shown in [12]. The calibration curves of the humidity sensor functionalized with CAB at different temperatures are presented in figure 9(b). One remarks a linear response from 20%R.H. to 60%R.H. with sensitivities of: 2.75 ± 0.1 fF/%R.H., 3.25 ± 0.1 fF/%R.H. and 3.44 ± 0.1 fF/%R.H. for 20 °C, 30 °C and 40 °C, respectively. The values have been calculated for incremental humidity changes. Hysteresis values, calculated as the maximum difference in output at any measurement within the sensor range (i.e. 0.2 pF), were found to be 4.5%, 4.5% and 3.5% for the 20 °C, 30 °C and 40 °C temperature conditions (figure 9(b)), respectively. Because of such slight hysteresis, mostly due to the much slower desorption kinetics of the sensor substrate, the decremental characteristics were shifted towards higher capacitances. Complete printed sensor characterization can be found in [11]. If higher precision and faster response are required, the substrate (PEN) parasitic sensitivity to humidity can be compensated by using a reference capacitor (i.e. other capacitive channel) [26, 27]. Moreover, a compact capacitor design such as a vertical capacitor configuration could be used to further decrease the response time [28–30], thanks to the complete elimination of the substrate response. It should be noted that the vertical structure (i.e. top and bottom electrodes) would be fully compatible with the current fabrication process involving two inkjetted layers of silver, although more complex fabrication process would be foreseen.

4.3. NH_3 vapor sensor characterization

Ammonia is a reducing gas and upon interaction with the PANI sensing layer, it deprotonates the emeraldine salt converting it to the emeraldine base form. This reduces the number of charge carriers (holes) in the sensing layer thus decreasing the electrical conductance. The process is reversible as by exposing the sensor to clean air, the resistance decreases to its initial values. The tests under controlled atmosphere (NH_3 and humidity) were performed in dynamic exposure between 0 ppm and 15 ppm, which is relevant for personal safety (i.e. TLV-TWA values ~30 ppm, country dependent), and at three different R.H. levels (i.e. 30%, 40% and 50%). The ammonia was supplied from a 50 ppm NH_3 in 5.5 synthetic air pressured bottle while saturated water vapour was obtained by purging synthetic air (5.5) through a large area babbler kept at constant temperature (25 °C). The required concentrations were realized by dynamic dilution in synthetic air with a computer controlled gas mixing system. Figure 10 shows in black (solid line, left axis) the relative changes in resistance of the PANI-based sensor with respect to its baseline resistance (R_0), and in blue (dotted-line, right axis) the relative capacitance changes for the humidity sensor. Although increasing the humidity level alters the baseline resistance value, it does not adversely affect, to a significant extent, the response and recovery of the sensor, over the ammonia concentration and humidity range studied here. The ammonia response of the polyaniline nanocomposite sensing material was proven to be less sensitive to varying humidity levels compared to the poly(4-styrenesulfonic acid)-doped PANI developed in our previous report [19]. In order to calculate the sensitivity to NH_3, the sensor was exposed at ammonia levels between 1 ppm and 25 ppm and at 30%R.H. (i.e. 1 h each step), as shown in figure 11(a). This resulted in a linear response with a relatively high sensitivity of 5.4

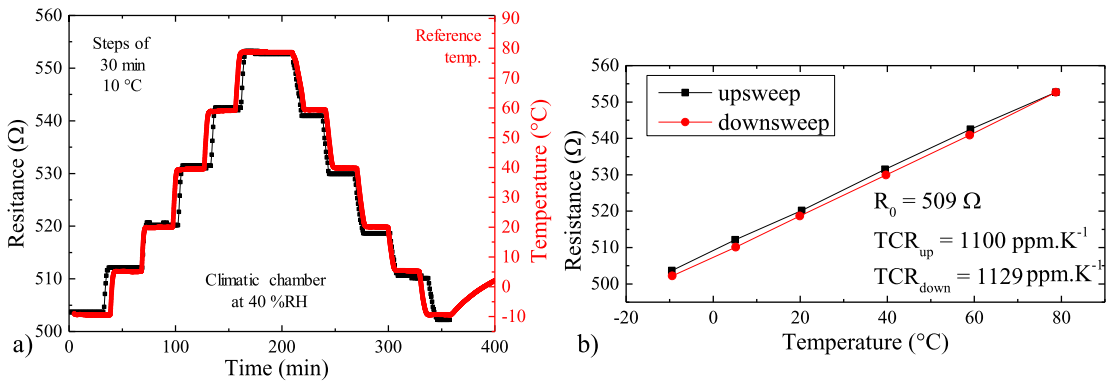

Figure 8. Smart label response to temperature. (a) The raw RTD response at 40%R.H. and (b) the calibration curves between −10 °C and 80 °C.

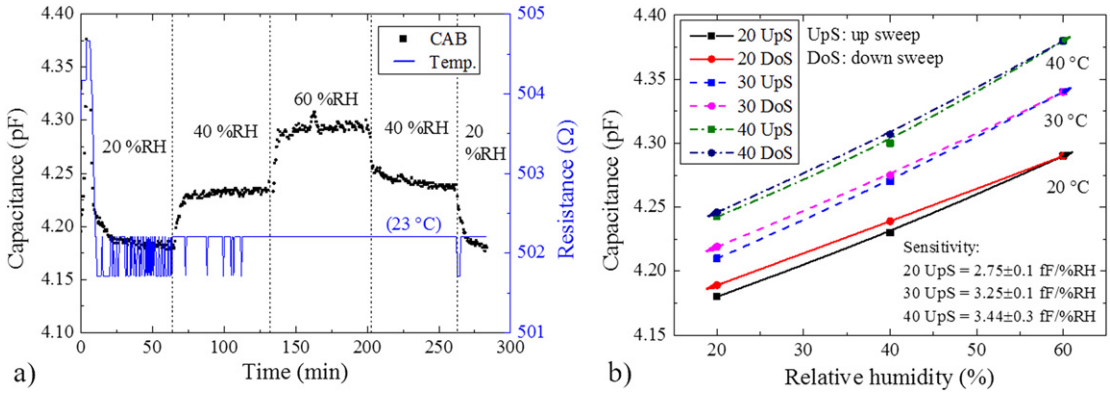

Figure 9. Humidity sensor characterization. (a) Dynamic characterization (up- and down-sweeps) for R.H. values between 20% and 60% and at room temperature: IDE capacitive transducer with CAB (black squares), reference IDE (red circles) and RTD measured resistance (blue solid line). (b) Humidity sensor calibration curves (up- and down-sweeps) for an R.H. range between 20% and 60% and temperature values of 20 °C, 30 °C and 40 °C.

± 0.2%/ppm for low ammonia concentrations, and a baseline of 6 MΩ, as shown in the inset of figure 11(a). The analogue signal from the resistive sensors was read out directly by the ADC of the microcontroller through a voltage divider (i.e. in the same way the RTD was interfaced) with matching resistance value in the range of MΩ.

In order to validate the operation of the micro hotplate when implemented in the tag architecture, a localized temperature step was applied while the response of the ammonia sensor was recorded using the developed smart label. The localized temperature change was used to quickly reset the chemical sensor after an ammonia exposure. As shown in figure 11(b), the test started with a 15 min stabilization cycle at a controlled value of humidity (40% R.H.), temperature (23 °C) and ammonia (0 ppm). Next, the platform was exposed to a step of 15 ppm of ammonia for 7 min. Finally, the micro hotplate was activated for 10 min. Figure 11(b) demonstrates the sensor recovery during the temperature pulse, which is faster compared to the room temperature desorption observed in figure 10 (i.e. after 1.5 h the signal returned to the baseline from 15 ppm to 0 ppm at 40% R.H.). As shown in [21], the theoretical detection limit of the ammonia sensor for the same structure used in this paper was lower than 100 ppb (i.e. at 95 °C). As presented, continuously localized heating decreases the recovery time, however, it deteriorates the sensor's detection limit and sensitivity [18], while considerably increasing the overall power consumption of the system.

The micro hotplate was directly connected to the main power supply (i.e. 150 mAh at 3.9 V battery—PK Cell from Adafruit) by means of a mechanical switch, which in turn generated a power of 50 mW across the 150 Ω resistor. Using the previously modelled Joule effect of such a configuration [18], the estimated temperature was found to be around 120 °C. Thanks to the thermal insulation of the transducers in the platform, the RTD reading remains invariant of the temperature changes in the micro hotplate.

Considering an active load of 12.8 mA (i.e. representing the power consumption of 50 mW when the heater is being activated), and a circuit load of 3.1 μA (i.e. representing the standby currents of the RFID chip (2 μA) and microcontroller (1.1 μA), the maximum lifetime of the system can be calculated as follows:

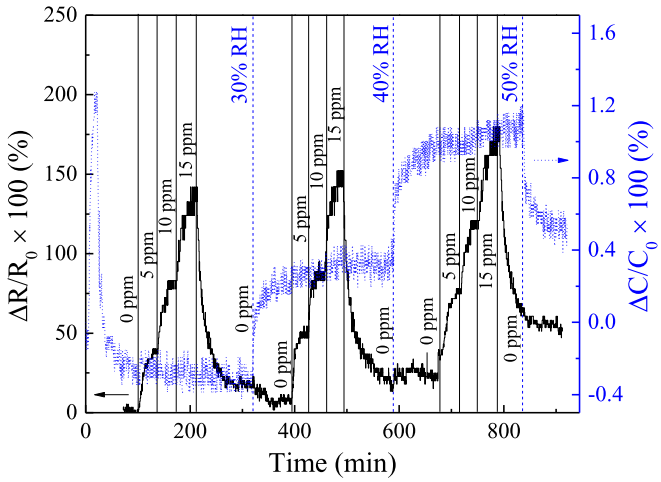

Figure 10. NH_3 sensor characterization. Dynamic sensor response for NH_3 levels between 0 ppm and 15 ppm (black solid line) and R.H. values of 30%, 40% and 50%. The humidity is also plotted as a blue-dotted line.

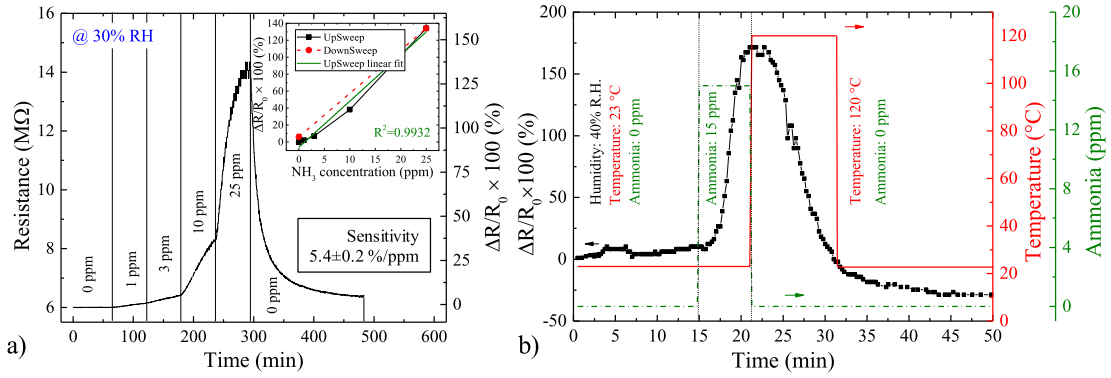

Figure 11. (a) Sensor response towards ammonia concentrations between 1 ppm and 25 ppm at 30% R.H. The corresponding sensitivity curve is shown in the inset. (b) Example of temperature pulse with the micro hotplate during ammonia sensing.

Table 1. Battery lifetime using typical system values.

Capacity	$Load_{passive}$	$Load_{circuit}$	T	P	Lifetime
150 mAh	3.1 μA	12.8 mA	30 s	60 min	57 days

$$\text{lifetime[h]} = \frac{\text{Capacity}_{bat}}{\text{Load}_{passive} + (\text{Load}_{circuit} * T/P)} \quad (2)$$

Where lifetime is given in hours, $Capacity_{bat}$ is the total battery capacity of the label, $Load_{passive}$ is the summation of the standby currents for the RFID and microcontroller, $Load_{circuit}$ is the maximum current of the system when operating the heater, T is the duration of the measurement and P is the periodicity of the measurement. Taking as an example the values in table 1, the lifetime is expected to be 57 days, which is compatible with standard requirements for the logistics industry.

Although the operation of the heater on tag has been demonstrated, the precise power control through temperature modulation needs to be optimized (i.e. applying short pulses of current to the heater) in order to improve sensor recovery and reduce power consumption.

5. Conclusion

The fabrication of an inkjet-printed multisensor platform and its integration onto a printed HF RFID smart label was presented. The label has the capability of measuring an RTD sensor, two capacitive sensors (demonstrated for humidity) and two resistive sensors (one of them demonstrated for NH_3). The platform was integrated through foil-to-foil techniques in order to interface it with a microcontroller and RFID chip

for retrieving and visualizing the measured/stored data. The integration technology developed here is a step forward in the production of cost effective smart sensing RFID labels using large-area and additive manufacturing techniques. Overall production costs are foreseen to be reduced by minimizing the number of Si components (i.e. ultimately just one application-specific integrated circuit) and replacing critical costly materials (i.e. gas permeable and dry film photoresist encapsulation). Such smart devices could be envisaged for application in the monitoring of perishable goods (food, medicine and biomaterials, among others) transported through a cold chain supply.

Acknowledgments

This work was funded by the EU FP7 project FlexSmell, a Marie Curie Initial Training Network (ITN), under the grant No. 238454.

References

[1] Koutsoumanis K 2009 Modelling food spoilage in microbial risk assessment *J. Food Protoc.* **72** 425–32
[2] Sutija D 2013 Printed sensor tag and smart objects *Proc. Energy Harvesting and Storage Europe* (*17–18 April Berlin, Germany*) pp 520–3
[3] Bozzi M *et al* 2013 Inkjet-printed antennas, sensors and circuits on paper substrate *IET Microwaves, Antennas Propag.* **7** 858–68
[4] Xiao S, Che L, Li X and Wang Y 2007 A cost-effective flexible MEMS technique for temperature sensing *Microelectronics J.* **38** 360–4
[5] Lee C-Y, Wu G-W and Hsieh W-J 2008 Fabrication of micro sensors on a flexible substrate *Sensors Actuators* A **147** 173–6
[6] Smits E, Schram J, Nagelkerke M, Kusters R, Heck G V, Acht V V, Koetse M M, van den Brand J, Gelinck G and Schoo H 2012 Development of printed RFID sensor tags for smart food packaging *Int. Meeting on Chemical Sensors* pp 403–6
[7] Humbert A, Tuerlings B J, Hoofman R J O M, Tan Z, Gravesteijn D, Pertijs M A P, Bastiaansen C W M and Soccol D 2013 A low-power CMOS integrated sensor for CO_2 detection in the percentage range *17th Int. Conf. on Solid-State Sensors, Actuators and Microsystems* pp 1649–52
[8] Salmeron J F, Molina-Lopez F, Rivadeneyra A, Vásquez Quintero A, Capitan-Vallvey L F, de Rooij N F, Banqueri Ozaez J, Briand D and Palma A J 2014 Design and development of sensing RFID Tags on flexible foil compatible with EPC Gen 2 *IEEE Sensors J.* **4** 4361–71
[9] Abad E, Zampolli S, Marco S, Scorzoni A, Mazzolai B, Juarros A, Gomez D, Elmi I, Cardinali G and Gomez J 2007 Flexible tag microlab development: gas sensors integration in RFID flexible tags for food logistic *Sensors Acuators* B **127** 2–7
[10] Briand D, Oprea A, Courbat J and Bârsan N 2011 Making environmental sensors on plastic foil *Mater. Today* **14** 416–23
[11] Molina-Lopez F, Briand D and de Rooij N F 2012 All additive inkjet printed humidity sensors on plastic substrate *Sensors Acuators* B **166-167** 212–22
[12] Molina-Lopez F, Vásquez Quintero A, Mattana G, Briand D and de Rooij N F 2013 Large-area compatible fabrication and encapsulation of inkjet-printed humidity sensors on flexible foils with integrated thermal compensation *J. Micromech. Microeng.* **23** 025012
[13] Wojkiewicz J L, Bliznyuk V N, Carquigny S, Elkamchi N, Redon N, Lasri T, Pud A A and Reynaud S 2011 Nanostructured polyaniline-based composites for ppb range ammonia sensing *Sensors Actuators* B **160** 1394–403
[14] Crowley K, Morrin A, Hernandez A, Omalley E, Whitten P, Wallace G, Smyth M and Killard A 2008 Fabrication of an ammonia gas sensor using inkjet-printed polyaniline nanoparticles *Talanta* **77** 710–7
[15] Vásquez Quintero A, van Remoortere B, Smits E C P, van den Brand J, Briand D, Schoo H F M and de Rooij N F 2013 Foil-to-foil lamination and electrical interconnection of printed components on flexible substrates *Microelectron. Eng.* **110** 52–8
[16] Chawla V and Ha D S 2007 An overview of passive RFID *IEEE Commun. Mag.* **45** 11–7
[17] Vásquez Quintero A, Briand D and de Rooij N F 2013 Effect of low-temperature processing on dry film photoresist properties for flexible electronics *J. Polym. Sci. Part* B **51** 668–79
[18] Danesh E, Molina-Lopez F, Camara M, Bontempi A, Vásquez Quintero A, Teyssieux D, Thiery L, Briand D, de Rooij N F and Persaud K C 2014 Development of a new Generation of ammonia sensors on printed polymeric hotplates *Anal. Chem.* **18** 8951–8
[19] Wessling B 2000 *Handbook of Nanostructured Materials and Nanotechnology* (Burlington, MA: Academic Press) pp 501–75
[20] Cao Y, Smith P and Heeger A J 1992 Counter-ion induced processibility of conducting polyaniline and of conducting polyblends of polyaniline in bulk polymers *Synth. Met.* **48** 91–7
[21] Danesh E and Persaud K C 2012 Flexible ammonia sensor based on polyaniline/carbon black composites operating at elevated temperatures *14th Int. Meeting on Chemical Sensors* (*Nuremberg*) pp 1134–6
[22] Sotzing G A, Phend J N, Grubbs R H and Lewis N S 2000 Highly sensitive detection and discrimination of biogenic amines utilizing arrays of polyaniline/carbon black composite vapor detectors *Chem. Mater.* **12** 593–5
[23] Chiang J-C and MacDiarmid A G 1986 'Polyaniline': Protonic acid doping of the emeraldine form to the metallic regime *Synth. Met.* **13** 193–205
[24] Tzou K and Gregory R V 1993 A method to prepare soluble polyaniline salt solutions—*in situ* doping of PANI base with organic dopants in polar solvents *Synth. Met.* **53** 365–77
[25] Vásquez Quintero A, Briand D and de Rooij N F 2015 Flip-chip integration of Si bare dies on polymeric substrates at low temperature using ICA vias made in dry film photoresist *J. Micromech. Microeng.* **25** 045013
[26] Oprea A, Courbat J, Bârsan N, Briand D, de Rooij N F and Weimar U 2009 Temperature, humidity and gas sensors integrated on plastic foil for low power applications *Sensors Actuators* B **140** 227–32
[27] Oprea A, Courbat J, Briand D, Bârsan N, Weimar U and de Rooij N F 2012 Environmental monitoring with a multisensor platform on polyimide foil *Sensors Actuators* B **171–172** 190–7
[28] Molina-Lopez F, Briand D, de Rooij N F and Smolander M 2012 Fully inkjet-printed parallel-plate capacitive gas sensors on flexible substrate 2012 *IEEE Sensors* pp 1–4
[29] Molina-Lopez F, Briand D and de Rooij N F 2015 Inkjet and microcontact printing of functional materials on foil for the fabrication of pixel-like capacitive vapor microsensors *Org. Electron.* **16** 139–47
[30] Vásquez Quintero A, Mattana G, Briand D and de Rooij N F 2013 Selft-standing printed humidity sensor with thermo-calibration and integrated heater *Proc. IEEE Transducers* pp 838–41